# Determination of LWP Aperture Dimensions

Matthew P. Garhart
*Computer Sciences Corporation*
29 September 1993

## Introduction

The effective LWP aperture dimensions (*i.e.*, length, width, and area) have been determined for both the large and small apertures. These values do not represent the true physical size of the apertures but rather the size as projected on the camera faceplate. Accurate measurements of the aperture dimensions are needed to properly calibrate trailed exposures (aperture length/width) and extended sources (aperture area).

Two methods were utilized to derive the large aperture area and both yielded similar results. The first analyzes trailed and point source fluxes using the method described by Garhart (1992a). The second is similar to the one developed by Panek (1982) and involves analysis of wavelength calibration (WAVECAL) images. This method was used successfully by Pérez and Loomis (1992) to derive the LWR large-aperture area. For a detailed discussion of the various methods and uncertainties involved in measuring the apertures see Pérez and Loomis (1991).

## Analysis of Trail-to-Point Flux Ratios

All images used in this study (listed in Tables 1 and 2) have been reprocessed using the final archive (NEWSIPS) software and are a subset of the low-dispersion sensitivity monitoring database. The analysis was performed on the extracted net spectrum before application of the absolute calibration. The data were corrected for temperature (THDA) induced sensitivity variations (Garhart 1991) and sections of the spectra affected by camera reseaux were interpolated across. Large-aperture trailed and point source spectra from several standard stars and within a given epoch (so as to eliminate camera sensitivity degradation effects) were averaged together. The average trailed and point source spectra were then ratioed to each other to provide a trail-to-point (T/P) net flux ratio for each time period and for each standard star, resulting in a total of 22 flux ratios for major axis trail length images and 5 flux ratios for minor axis trail length data.

The trail path distance can be expressed as follows:

$$Trail\ Distance = Trail\ Rate \times R_\lambda \times t_{PT}$$

where $Trail\ Rate$ is in arcseconds per second, $R_\lambda$ is the T/P flux ratio, and $t_{PT}$ is the effective point source exposure time in seconds after correcting for OBC quantitization (Oliversen 1991) and camera rise time effects (González-Riestra 1991). The trail rates and the effective

point source exposure times are known quantities (Tables 1 and 2), therefore one can derive a trail path measurement by calculating $R_\lambda$. A set of trail lengths as a function of wavelength were determined for each of the 22 T/P ratios and found to be in agreement, so the results were averaged to produce a final major axis trail length measurement. Following the method of Panek (1982), the data were then binned at 50Å wavelength intervals and a mean value was determined. The same procedure was performed on the minor axis trail length data using an average of 5 T/P flux ratios.

The LWP major axis trail length as a function of wavelength is plotted in Figure 1a. Unlike the SWP trail length analysis (Garhart 1992a), no wavelength dependency is seen. The minor axis trail length analysis is displayed in Figure 1b and, as is the case with the major axis, no wavelength dependency is evident. The mean values and the corresponding standard deviations (Table 4) are calculated using a wavelength range of 2000–3200Å.

According to Panek (1982), the large-aperture width is ~1.8 percent smaller than the trail length across the short axis and the large-aperture length is ~0.8 percent larger than the trail length across the long axis due to the 14 degree tilt of the FES with respect to the major and minor axes. In addition, the large-aperture area is smaller than the product of the major and minor axes lengths because of the rounded aperture edges. The aperture area correction factor was derived for the long wavelength cameras using the method described by Garhart (1992b) and is similar to the number quoted by Panek (1982). A pre-flight photograph of the long wavelength large and small apertures is shown in Figure 2. The aperture dimensions, derived using these corrections, are listed in Table 4.

# Analysis of Wavelength Calibration Data

This method involves the examination of monochromatic images of the apertures. These types of images can be obtained from WAVECAL exposures taken with the aperture mechanism left open, thus simultaneously illuminating both the large and small apertures. This technique assumes that the light from the Pt-Ne lamps is collimated and that the illumination over the apertures is uniform. The first assumption is true because the distance between the aperture plate and the WAVECAL lamps is large compared with the size of the apertures. The second assumption is proven to be true from the T/P flux ratio analysis.

The image chosen for this study (LWP 7834) was processed using the NEWSIPS processing software (Figure 3a). The image was rotated such that the orders are horizontal and the photometric correction applied. Each of the emission lines represents a projection of the aperture onto the camera faceplate. The effective large-aperture area in square pixels is found by ratioing the total flux of the line to the mean central flux. The ratio is converted to square arcseconds by applying the plate scale (1.51"/pixel). The total flux of the emission line is found by summing the FN contained within a rectangle ($\sim 12 \times 20$ pixels) encompassing the large-aperture emission feature. Care was taken to ensure that no flux fell outside

the rectangle before summation. The mean central flux is the average FN of a rectangular box of pixels ($\sim 4 \times 8$) centered about the middle of the emission feature. The average background, determined from a $12 \times 12$ box of pixels, was subtracted from the FN data in each case before performing any calculation. An example of the procedure is illustrated by Figure 3b. A total of 32 emission features (tabulated in Table 3) were measured to produce an average large-aperture area (Table 4).

The area of the small aperture was arrived at using a similar method. Pairs of large- and small-aperture emission lines were found and the total small-aperture flux, with a correction for the background, was measured. The ratio of the total flux in the large and small apertures is then the ratio of the aperture areas. Dividing the large-aperture area for a particular large-small pair by this large-to-small ratio yields a measurement of the small-aperture area. A total of 20 small-aperture emission lines (tabulated in Table 3) were used to determine the aperture area (Table 4).

# Conclusion

The calibration group recommends the adoption of the large- and small-aperture dimensions as derived from the WAVECAL analysis. Although the large-aperture area results from the two methods are in very close agreement (within one sigma), the area determined from WAVECALs is preferred as it represents the true projection of the aperture on the camera faceplate.

# References


Bohlin, R.C., et al. 1980, A&A, 85, 1

Garhart, M.P. 1991, *Record of the IUE Three Agency Coordination Meeting*, June 1991, p. VI-38

Garhart, M.P. 1992a, IUE NASA Newsletter, No. 48, 88

Garhart, M.P. 1992b, IUE NASA Newsletter, No. 49, 22

González-Riestra, R. 1991, *Record of the IUE Three Agency Coordination Meeting*, June 1991, p. VI-82

Oliversen, N.A. 1991, IUE NASA Newsletter, No. 45, 56

Panek, R. 1982, IUE NASA Newsletter, No. 18, 68

Pérez, M. and Loomis, C. 1991, *Record of the IUE Three Agency Coordination Meeting*, June 1991, p. VI-11

Pérez, M. and Loomis, C. 1992, *Record of the IUE Three Agency Coordination Meeting*, June 1992, p. III-41

Table 1a: LWP Images Used in Aperture Length Analysis

| Object | Trailed Image no. | Pt. Source Image no. | Date | Trail Rate ($\frac{arcsec}{sec}$) | $t_{PT}$ $(sec)$ |
|---|---|---|---|---|---|
| HD 60753 | 1667 | 1690 | 1982.8 | 0.7798 | 5.6110 |
| | 1671 | 1713 | | | |
| | 1674 | | | | |
| | 4171 | 4122 | 1984.7 | | |
| | 4224 | 4172 | | | |
| | 4228 | | | | |
| | 4232 | | | | |
| | 6799 | 6808 | 1985.7 | | |
| | 6804 | 6809 | | | |
| | 6806 | | | | |
| | 10973 | 10887 | 1987.4 | | |
| | 10977 | 10899 | | | |
| | 10983 | | | | |
| | 15038 | 15053 | 1989.1 | | |
| | 15041 | 15062 | | | |
| | 15105 | 15107 | 1989.2 | | |
| | 15106 | 15135 | | | |
| | 15110 | | | | |
| | 19701 | 19629 | 1991.1 | | |
| | 19706 | 19635 | | | |
| | | 19636 | | | |
| | | 19709 | | | |
| BD+75° 325 | 2932 | 2767 | 1984.2 | 0.1994 | 19.538 |
| | 2934 | 2933 | | | |
| | 4121 | 4240 | 1984.7 | | |
| | 4136 | 4568 | | | |
| | 4182 | | | | |
| | 16956 | 17086 | 1990.0 | | |
| | 17119 | 17104 | | | |
| | 20152 | 20153 | 1991.3 | | |
| | 20287 | 20282 | | | |
| | 21789 | 21788 | 1991.9 | | |
| | 21907 | 21903 | | | |
| | | 21908 | | | |
| | | 21942 | | | |

Table 1b: LWP Images Used in Aperture Length Analysis

| Object | Trailed Image no. | Pt. Source Image no. | Date | Trail Rate ($\frac{arcsec}{sec}$) | $t_{PT}$ ($sec$) |
|---|---|---|---|---|---|
| BD+28° 4211 | 3539 | 3538 | 1984.4 | 0.0990 | 49.848 |
| | 3604 | 3688 | | | |
| | 6040 | 6039 | 1985.4 | | |
| | 6104 | 6103 | | | |
| | | 6147 | | | |
| | 6674 | 6672 | 1985.6 | | |
| | 6676 | 6673 | | | |
| | 8991 | 8985 | 1986.7 | | |
| | 8992 | 8989 | | | |
| | | 8990 | | | |
| | 21780 | 21779 | 1991.9 | | |
| | 21929 | 21928 | | | |
| HD 93521 | 2486 | 2484 | 1984.0 | 1.8012 | 2.744 |
| | 2554 | 2553 | | | |
| | 2871 | 2768 | 1984.2 | | |
| | 2936 | 2935 | | | |
| | 5237 | 5082 | 1985.0 | | |
| | | 5220 | | | |
| | 21762 | 21761 | 1991.9 | | |
| | 21909 | 21910 | | | |
| | 25598 | 25597 | 1993.4 | | |
| | | 25731 | | | |

Table 2: LWP Images Used in Aperture Width Analysis

| Object | Trailed Image no. | Pt. Source Image no. | Date | Trail Rate ($\frac{arcsec}{sec}$) | $t_{PT}$ ($sec$) |
|---|---|---|---|---|---|
| BD+28° 4211 | 25999 | 26000 | 93.6 | 0.1821 | 49.848 |
| HD 93521 | 24726 | 24725 | 93.0 | 3.04 | |
| HD 60753 | 22929 | 22930 | 92.3 | 1.52 | 5.611 |
| | 24711 | 24710 | 93.0 | | |
| BD+75° 325 | 24713 | 24712 | 93.0 | 0.456 | 19.538 |

Table 3: Results of WAVECAL Analysis

| (X,Y) | BKGD | Total LGAP | Center Flux | Ratio | LGAP Area | Total SMAP | LG/SM Ratio | SMAP Area |
|---|---|---|---|---|---|---|---|---|
| 639,170 | 209.52 | 259581 | 2630.4 | 98.69 | 225.01 | | | |
| 390,220 | 341.04 | 254478 | 3051.3 | 83.40 | 190.16 | | | |
| 685,229 | 236.65 | 456638 | 4874.8 | 93.67 | 213.58 | | | |
| 689,258 | 235.42 | 731098 | 7559.5 | 96.71 | 220.51 | 20555 | 35.57 | 6.20 |
| 350,315 | 370.58 | 347280 | 4152.7 | 83.63 | 190.68 | | | |
| 479,341 | 436.68 | 224312 | 2576.3 | 87.07 | 198.52 | 8667.5 | 25.88 | 7.67 |
| 527,341 | 399.33 | 571553 | 6741.6 | 84.78 | 193.31 | 19325 | 29.58 | 6.54 |
| 424,342 | 426.90 | 242252 | 2594.9 | 93.36 | 212.86 | | | |
| 473,360 | 586.97 | 679567 | 8092.7 | 83.97 | 191.47 | 21325 | 31.87 | 6.01 |
| 96,370 | 142.45 | 816160 | 8632.7 | 94.54 | 215.57 | 29173 | 27.98 | 7.71 |
| 140,390 | 178.27 | 238343 | 2736.9 | 87.09 | 198.56 | 6168.8 | 38.64 | 5.14 |
| 615,411 | 363.74 | 340918 | 4089.6 | 83.36 | 190.07 | 13414 | 25.42 | 7.48 |
| 155,422 | 234.30 | 279052 | 3143.7 | 88.77 | 202.39 | 8124.5 | 34.35 | 5.89 |
| 508,422 | 625.96 | 446947 | 5314.6 | 84.10 | 191.75 | | | |
| 578,456 | 551.92 | 569255 | 6335.6 | 89.85 | 204.87 | 16872 | 33.74 | 6.07 |
| 318,468 | 620.10 | 198648 | 2265.8 | 87.67 | 199.90 | | | |
| 574,468 | 548.94 | 372675 | 4230.0 | 88.10 | 200.88 | | | |
| 582,480 | 509.00 | 1097530 | 12401 | 88.50 | 201.80 | | | |
| 91,493 | 348.33 | 387904 | 4501.3 | 86.18 | 196.49 | 13063 | 29.70 | 6.62 |
| 341,493 | 527.27 | 445952 | 5208.2 | 85.63 | 195.23 | | | |
| 648,504 | 551.10 | 462002 | 5277.2 | 87.55 | 199.62 | 18221 | 25.36 | 7.87 |
| 186,506 | 357.33 | 475747 | 5260.7 | 90.43 | 206.20 | 12059 | 39.45 | 5.23 |
| 142,518 | 336.14 | 453402 | 5116.9 | 88.61 | 202.04 | 13642 | 33.24 | 6.08 |
| 152,575 | 293.88 | 241534 | 2635.1 | 91.66 | 208.99 | | | |
| 633,588 | 238.30 | 417071 | 4534.2 | 91.98 | 209.73 | 12340 | 33.80 | 6.21 |
| 499,604 | 417.95 | 332680 | 3735.7 | 89.05 | 203.05 | 12421 | 26.78 | 7.58 |
| 342,620 | 292.88 | 415255 | 4544.6 | 91.37 | 208.34 | | | |
| 336,652 | 202.95 | 218220 | 2538.5 | 85.96 | 196.01 | 5877.4 | 37.13 | 5.28 |
| 265,653 | 173.50 | 443205 | 4650.9 | 95.29 | 217.28 | 11085 | 39.98 | 5.43 |
| 517,653 | 197.44 | 1033080 | 10925 | 94.56 | 215.61 | 29174 | 35.41 | 6.09 |
| 271,670 | 167.27 | 306361 | 3371.5 | 90.87 | 207.19 | 9091.9 | 33.70 | 6.15 |
| 413,686 | 81.84 | 228642 | 2651.3 | 86.24 | 196.63 | 5946.7 | 38.45 | 5.11 |

Table 4: LWP Aperture Dimensions

| **Garhart** | **Panek** | **Bohlin** | **Dimension** |
|---|---|---|---|
| 21.84±0.39 | 20.5±1.0 | | Major Axis Trail Length (arcsec) |
| 22.51±0.40 | 20.7±1.0 | < 23.8 | Large-Aperture Length (arcsec) |
| 10.21±0.18 | 9.5±0.1 | | Minor Axis Trail Length (arcsec) |
| 9.91±0.17 | 9.3±0.1 | < 10.2 | Large-Aperture Width (arcsec) |
| 0.92±0.01 | 0.91 | | Large-Aperture Area Correction |
| 205.23±5.07 | 175.0±10.0 | <221.0 | Large Aperture Area from T/P ratios (arcsec$^2$) |
| 203.26±9.28 | 203.0±6.0 | | Large Aperture Area from $\lambda$CAL image (arcsec$^2$) |
| 32.62±4.64 | 29.5±1.5 | 17.8 | Large-to-Small Aperture Ratio |
| 6.32±0.86 | 5.93 | 12.42 | Small Aperture Area (arcsec$^2$) |
| 2.84±0.07 | 2.75 | 3.98 | Small Aperture Diameter (arcsec) |

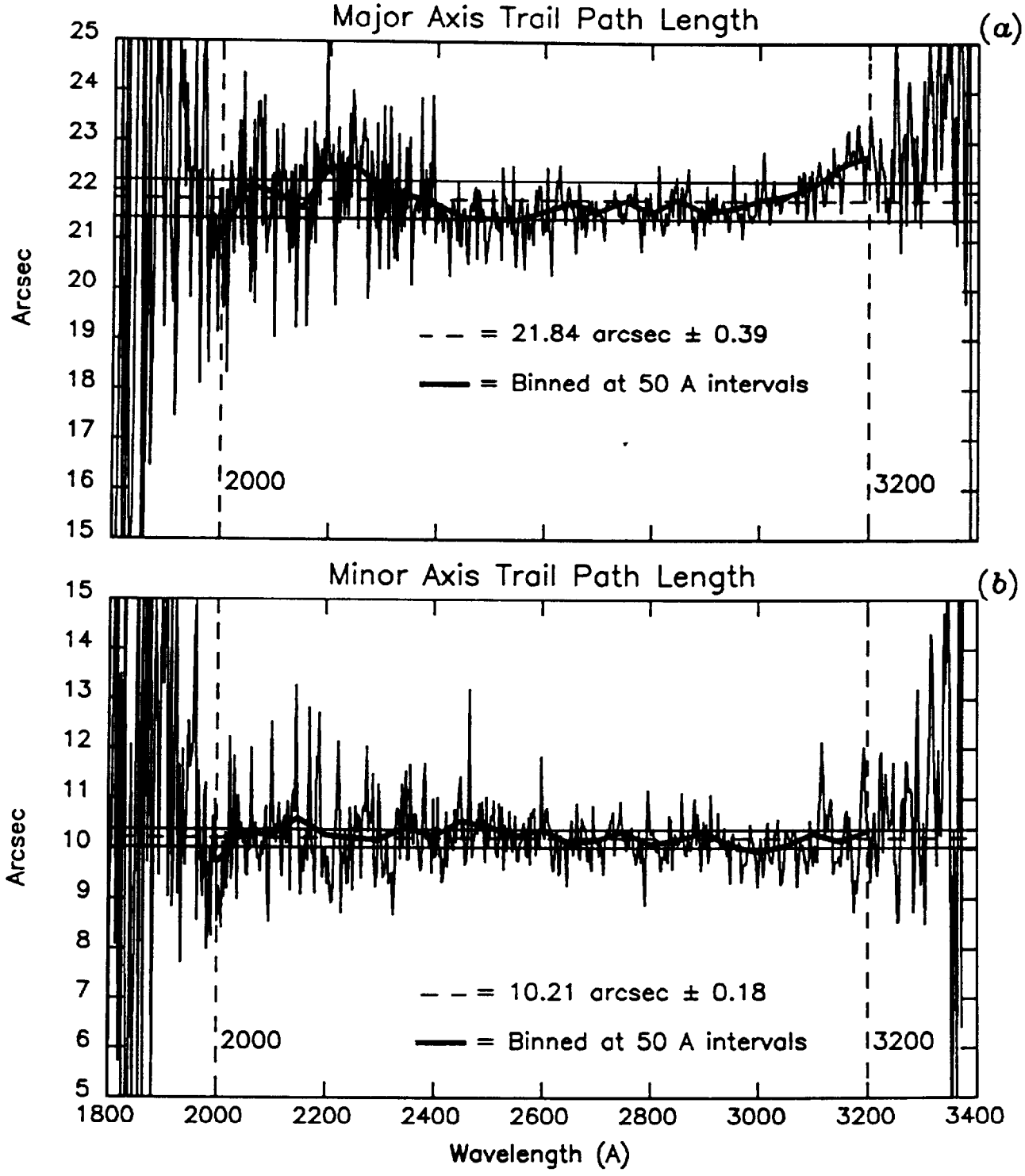


Figure 1: Panel *a* shows the major axis trail path length. Panel *b* shows the minor axis trail path length.

Figure 2: Digitized image of a pre-flight photograph of the long wavelength apertures. Dark blob in the middle is a dust mote.

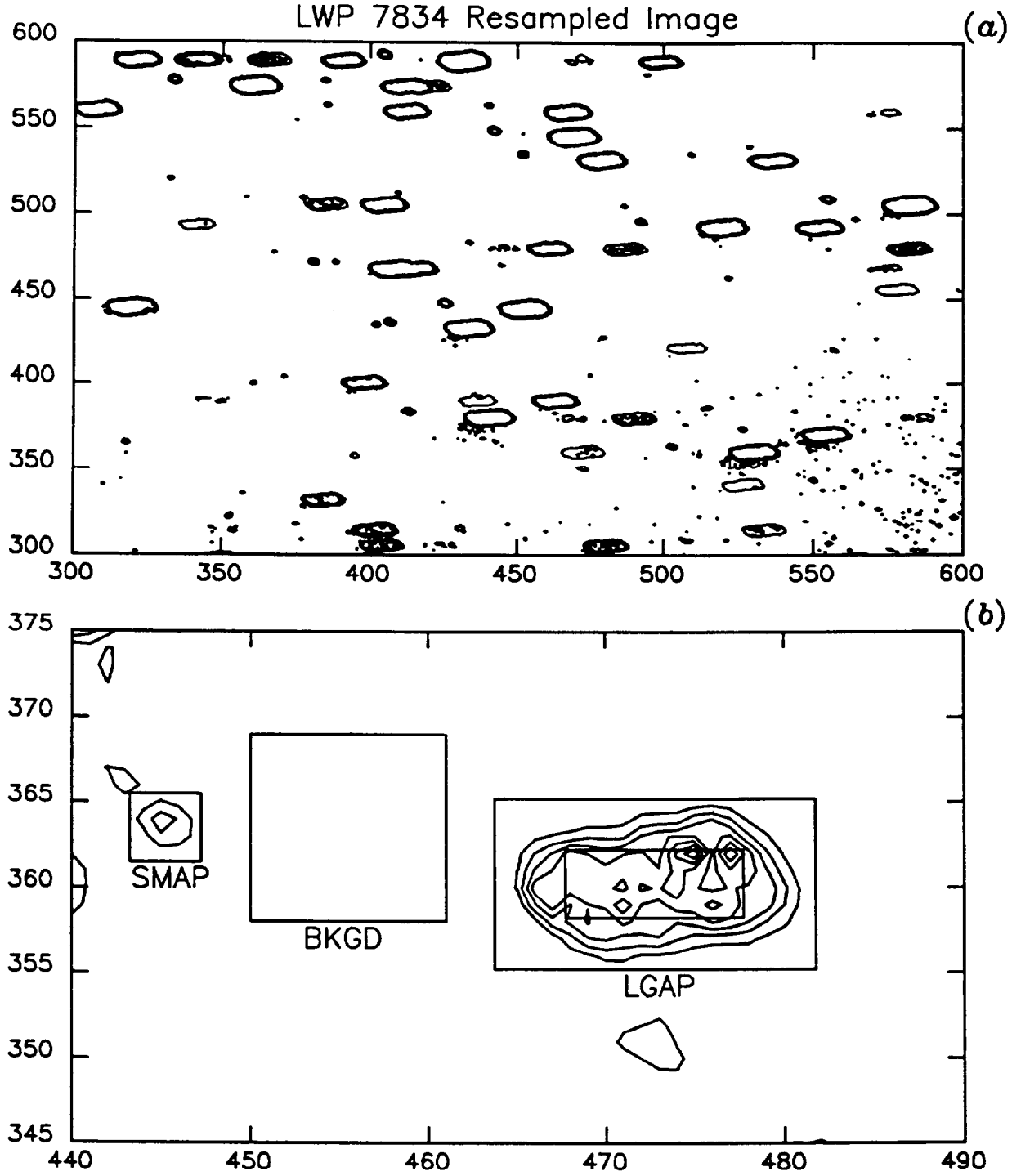


Figure 3: Panel *a* shows a section of the camera faceplate for a WAVECAL image. Panel *b* shows an expanded view of a small- and large- aperture Pt-Ne emission feature.